Available online at www.sciencedirect.com
ScienceDirect
Trans. Nonferrous Met. Soc. China 25(2015) 2272−2278
Transactions of Nonferrous Metals Society of China
www.tnmsc.cn

Synthesis and characterization of $ZnTiO_3$ with high photocatalytic activity

Xin YAN[1], Cui-lian ZHAO[1], Yi-long ZHOU[1], Zhen-jun WU[1], Jian-min YUAN[2], Wen-sheng LI[1]

1. College of Chemistry and Chemical Engineering, Hunan University, Changsha 410082, China;
2. College of Materials Science and Engineering, Hunan University, Changsha 410082, China

Received 29 March 2014; accepted 30 September 2014

Abstract: Perovskite $ZnTiO_3$ was prepared through a new method which contained a hydrothermal process for the preparation of titanate nanotubes and an ion-exchange process. The titanate nanotubes were inferred to be $H_2Ti_3O_7{\cdot}3H_2O$. X-ray diffraction (XRD) result revealed the presence of cubic perovskite phase of $ZnTiO_3$. The unique chain-like morphology of $ZnTiO_3$ was observed by scanning electron microscopy (SEM) and transmission electron microscopy (TEM). UV−Vis diffusive reflection spectra of $ZnTiO_3$ indicated that the absorbance obviously increased in the visible light region. The degradation rate of methyl orange solution (15 mg/L) reached 95.3% over $ZnTiO_3$ (0.3 g/L) after 20 min xenon light irradiation, which was higher than that using the commercial catalyst P25 under the same reaction condition. The degradation kinetic results follow the first-order equation and the rate constant is 0.1020.
Key words: $ZnTiO_3$; ion-exchange; photocatalysis; perovskite; synthesis; characterization

1 Introduction

The removal of organic pollutants in wastewater is a huge task in environmental protection, because they have led to serious contamination in many countries worldwide. Photosensitized degradation on an applicable catalyst has been proven to be the most widely used method. Therefore, searching for a catalyst with high efficiency has caught much attention [1,2] for good piezoelectric properties [3], catalytic properties and damping properties [4]. Since the phase equilibriums of a $ZnO{-}TiO_2$ system were reported by DULIN and RASE in the 1960s [5], some unique physical and chemical properties of perovsktite-type $ZnTiO_3$ have been investigated, such as the low band gap (2.88 eV), high dielectric constant ($\varepsilon\approx19$), high quality factor (Q=3000), and small temperature coefficient of the resonant frequency ($\tau_f=55\times10^{-6}$/°C) [6]. $ZnTiO_3$ plays an important role in photocatalysis [7], microwave dielectric material [6], gas sensor [8] and desulphurization [9].

$ZnTiO_3$ partially decomposes into Zn_2TiO_4 and rutile at about 945 °C [10]. Methods for preparing perovskite materials at lower temperatures include adding a glass phase [11], a sol−gel process [12,13], pulsed-laser deposition (PLD) technique [14], etc. Nevertheless, adding a glass phase lowers the stability factor and tolerance factor, which is attributed to the presence of impure $ZnTiO_3$ [15]. In addition, preparing $ZnTiO_3$ by a sol−gel process consumes expensive soluble Ti^{4+} salts such as $TiCl_4$ and $Ti(OC_2H_5)_4$ as raw materials, thus increasing the manufacturing cost. Pulsed-laser deposition (PLD) technique reacts on substrates, which is used for preparing thin films. Ion-exchange with titanate nanotubes is an attractive method for doping titanate nanotubes [16,17]. Multilayer titanate nanotubes displayed a high ion-exchange activity and $CoTiO_3$ was synthesized by the ion-exchange method using titanate nanotubes at lower temperatures [18]. It has shown a new method to prepare perovskite compounds at low temperature, which just uses TiO_2 and metallic salts as raw materials.

In this work, $ZnTiO_3$ nanocomposites were successfully synthesized by a method that combined a hydrothermal process for the preparation of titanate nanotubes [19] with an ion-exchange process for the exchange of Zn^{2+} with H^+. Due to the electron-capture capacity, Zn^{2+} was used for ion-exchange with H^+ in the perovskite structure to enhance the electron−hole separation efficiency. This synthesis strategy for the preparation of the material is low raw material cost and simple operation than traditional methods. Herein, we

Foundation item: Projects (50702020, 81171461) supported by the National Natural Science Foundation of China; Project (11JJ4013) supported by Natural Science Foundation of Hunan Province, China; Project supported by the Young Teacher Promotion Fund by Hunan University, China
Corresponding author: Zhen-jun WU; Tel/Fax: +86-731-85956121; E-mail: wooawt@163.com
DOI: 10.1016/S1003-6326(15)63841-9

firstly synthesized the chain-like $ZnTiO_3$ material with high surface area and thus enhanced the surface properties of the material. Because of the introduction of Zn^{2+} and the special morphology, the photocatalyst showed good photocatalytic performance, which was investigated by the degradation rate of methyl orange under the irradiation of xenon light.

2 Experimental

2.1 Sample preparation

Titanate nanotubes were synthesized by hydrothermal treatment in alkaline solution [20]. Firstly, 10 mol/L NaOH was added into the rutile powder and then autoclaved at 120 °C for 24 h. Secondly, the slurry was rinsed with deionized water until the pH value reached 8. After being filtrated and dried, the obtained titanate nanotube powders were characterized by the inductively coupled plasma−atomic emission spectrometry (ICP−AES, Baird PS−6) to detect the content of Ti in the titanate nanotubes. $Zn(NO_3)_2{\cdot}4H_2O$ and the titanate nanotube powers were mixed in water in the stoichiometric ratio of 1:1. The mixture was strirred and heated to 80 °C after adjusting the pH value to 6. The final precipitates were washed with deionized water several times to avoid the physical adsoption of Zn^{2+} and NO_3^-. The solid product was filtrated and dried, followed by calcination at 700 °C for 3 h in air. After being ground, the catalyst powder was obtained.

2.2 Characterization

Thermogravimetric analysis (TGA) and differential scanning calorimetry (DSC) analysis of precursor powders were conducted by a thermoanalyser (NETZSCH STA 409 PC/PG) in nitrogen atmosphere over the temperature range of 30−1100 °C at a constant heating rate of 10 °C/min. The phase and crystal structure were characterized by X-ray diffraction (XRD, Rigaku D/Max 2500) using Cu K_α (λ=1.542 Å) radiation in the scan range from 5° to 80°. The microstructure of the products was detected by filed-emission scanning electron microscopy (FESEM, JSM 6700F) and transmission electron microscopy (TEM, Tecnai G^2 F20 S-Twin). UV−Vis diffuse reflectance spectra (DRS) were recorded on a UV−Vis spectrophotometer (Cary 300, USA) with an integrating sphere.

2.3 Photoactivity evaluation

The photodegradation of aqueous methyl orange was carried out in a 250 mL pyrex glass vessel under a 500 W xenon lamp. Aqueous suspensions of methyl orange (250 mL) were placed in a vessel and the photocatalyst was added. Prior to irradiation, the suspensions were magnetically stirred in dark condition for 10 min to establish adsorption−desorption equilibrium. At certain time intervals, 8 mL aliquots were sampled and centrifuged to remove the particles. The filtrates were analyzed by recording variations of the maximum absorption peak (465 nm for methyl orange) using a Shimadzu UV−1800 spectrophotometer.

3 Results and discussion

3.1 Characterization of protonated titanates

Figure 1 shows the XRD pattern of the protonated titanates. No standard pattern can be found in powder diffraction file (PDF) cards that matches with the XRD pattern of protonated titanates in Fig. 1. The XRD pattern of protonated titanate is similar to the results of many other researches [16,21,22], in which $H_2Ti_3O_7{\cdot}nH_2O$ has been certified. In order to determine the value of n, protonated titanates were dissolved in sulfuric acid (103 mg/L) to detect the content of Ti element by the ICP-AES, the result was 47.4 mg/L, which revealed that the content of Ti element in $H_2Ti_3O_7{\cdot}nH_2O$ was 46.02%. Furthermore, the Ti content in $H_2Ti_3O_7{\cdot}3H_2O$ was 46.08%. Therefore, the chemical composition of titanate nanotube was represented as $H_2Ti_3O_7{\cdot}3H_2O$.

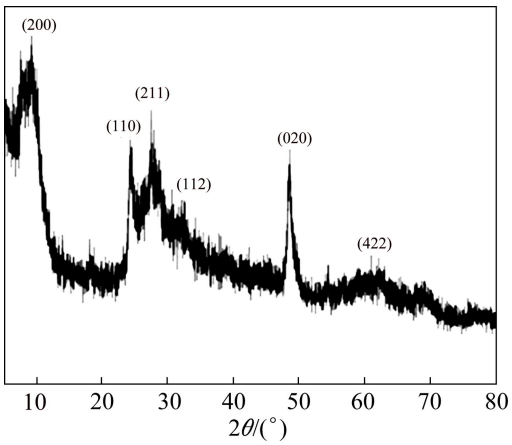

Fig. 1 XRD pattern of protonated titanates

Figure 2 show typical transmission electron microscopy (TEM) images of the as-prepared $H_2Ti_3O_7{\cdot}3H_2O$ at low and high magnifications, respectively. The size of the randomly aligned and high dispersed $H_2Ti_3O_7{\cdot}3H_2O$ shown in Fig. 2(a) is about 20 nm in width and several nanometers in length. More detailed information of the structure presented in the high-magnification TEM image is shown in Fig. 2(b), which indicated that $H_2Ti_3O_7{\cdot}3H_2O$ nanotubes showed a layer structure and tube shape. By observing the interior of $H_2Ti_3O_7{\cdot}3H_2O$ nanotubes (Fig. 2(b)), we can see that the tube thickness is uneven, which is different from the result in many researches [23,24]. ZHANG et al [25] reported the formation mechanism of $H_2Ti_3O_7$ nanotubes

and pointed out that the multiwall spiral nanotubes were transformed from the uneven sheets for the asymmetrical environment. It might be the reason for the uneven tube thickness. It is of vital importance for the preparation of the final product to synthesize the $H_2Ti_3O_7·3H_2O$ with layered and tubular structure, which displays good ion-exchange property [18,26,27].

3.2 Characterization of prepared $ZnTiO_3$

Figure 3 shows the TG/DSC curves of the zinc titanate precursor powders after vacuum drying treatment at 40 °C for 12 h. The shape of the TG curve is similar to that of the titanate nanotube reported by YANG and SWISHER [28]. The mass loss rate below 100 °C is about 5.8 %, which is attributed to evapration of surface adsorbed water. The mass loss from 100 °C to 300 °C is due to the loss of hydroxyl (—OH) groups between layers [29] and the mass loss from 300 °C to 570 °C is ascribed to the loss of —OH groups between layers, corresponding to a DSC exothermic peak at 237 °C and a broad exothermic peak, respectively. It reveals that the product consists of a great deal of hydroxyl structures between the layers. These explanations are reasonable considering the layered structure of nanotubes [18]. The sample mass changes little after 570 °C and the weak DSC peak at 614 °C should be a transition to crystalline phase. According to the above analysis, titanate nanotubes display a layered structure with —OH groups. Furthermore, the —OH groups disappear after 570 °C and return to a thermal stable structure. It is suggestive that $ZnTiO_3$ may be synthesized above 600 °C. This point is further addressed in the following three different synthetic processes.

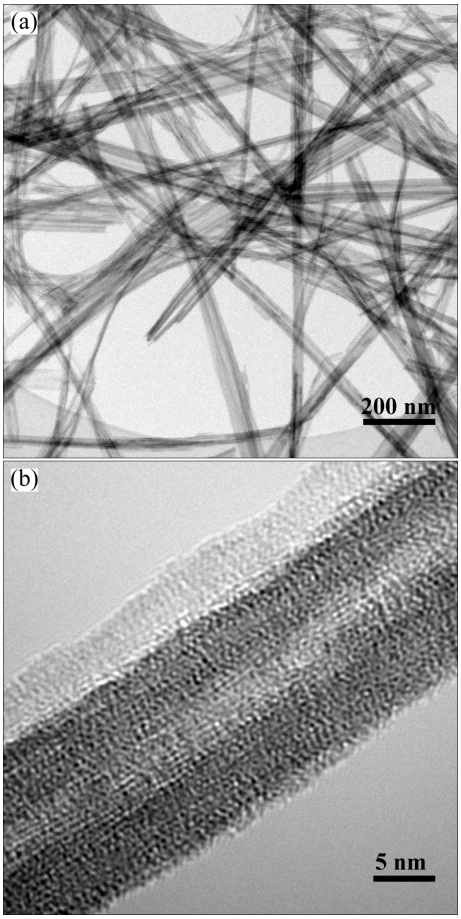

Fig. 2 TEM images of $H_2Ti_3O_7·3H_2O$ nanotube structures: (a) Low magnification; (b) High magnification

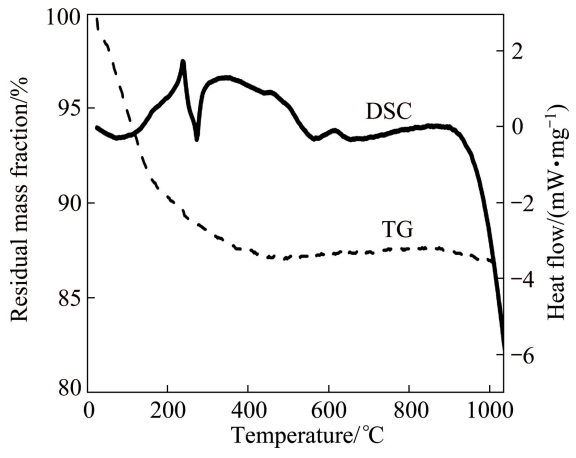

Fig. 3 Results of thermal analysis of zinc titanate precursor

Figure 4 shows the XRD patterns of the zinc titanate precursor powders calcined at different temperatures for 3 h. On the basis of the TG and DSC investigations, we studied samples calcined from 600 °C to 750 °C. At 600 °C, the XRD pattern shows the presence of anatase, due to the reflection peaks located at (220), (311), (511) and (440) (JCPDS card No. 39−0190, unit cell $a=b=c=$ 8.408 Å). However, samples calcined at 600 °C for 3 h have shown the coexistence of ZnO, Zn_2TiO_4, and anatase. KRYLOVA et al [30] have reported that the TiO_2 and Zn_2TiO_4 are decomposed from $Zn_xTi_yO_z$, which is regarded as the intermediate in this work. The samples heat-treated at 700 °C for 3 h exhibit the pure crystalline phase of $ZnTiO_3$ without any peaks from the other impurity. When the temperature increases to 750 °C,

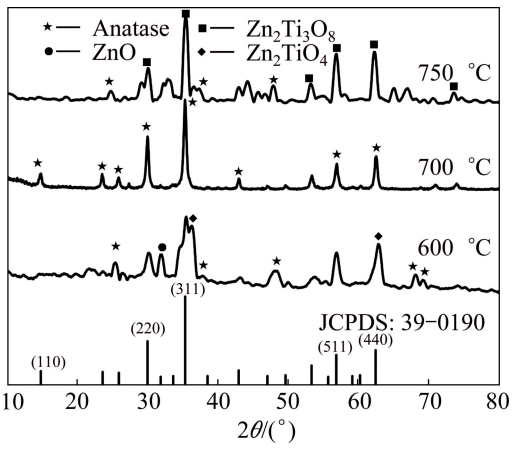

Fig. 4 XRD patterns of samples calcinated in air at different temperatures

several peaks related to $Zn_2Ti_3O_8$ (JCPDS card No. 39−0190) and anatase appear. YANG and SWISHER [28] have pointed out that $Zn_2Ti_3O_8$ is a thermodynamically stable compound up to temperature between 700 °C and 800 °C. Therefore, the better temperature to synthesize $ZnTiO_3$ is at 700 °C. The reaction of $ZnTiO_3$ can be represented by the following equation:

$$Zn(NO_3)_2{\cdot}4H_2O+H_2Ti_3O_7{\cdot}3H_2O \rightarrow Zn_xTi_yO_z \rightarrow ZnTiO_3 \quad (1)$$

Figure 5 shows the SEM and TEM images of $ZnTiO_3$ specimens after a solid-state treatment at 700 °C for 3 h. The shape of $ZnTiO_3$ is similar to chain. These chain-like $ZnTiO_3$ nanocomposites do not present a hollow structure, and the primary layer structure of titanate nanotubes has also been replaced by a chain-like structure with many nodes. According to the TEM image shown in Fig. 5(b), there is no clear boundary between two nodes. That is to say, the chains are not formed by simple arrangement of particles but a whole structure.

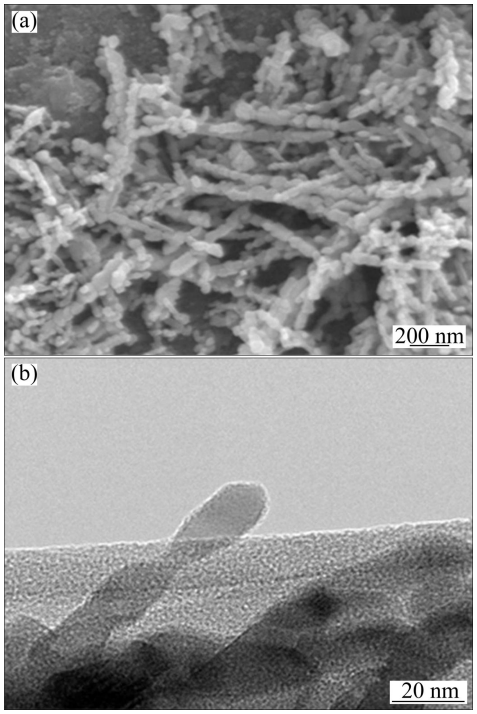

Fig. 5 SEM (a) and TEM (b) images of chain-like $ZnTiO_3$ specimens

Regarding to the formation of chain-like structure of $ZnTiO_3$, it formed in the final calcination process, because the nanotube structure still remained after ion-exchange without other external forces [18]. A great deal of hydroxyl groups between the layers released during the heating process, resulting in the partial collapse of the nanotubes. This explanation agrees well with the TG and DSC analyses shown in Fig. 3. On the other hand, the zinc ions can improve the stability of titanate nanotubes for its bigger radius than H. Figure 5(b) shows that the nanotubes subsided partly, resulting in the chain-like structure of $ZnTiO_3$.

3.3 UV−Vis diffuse reflection spectra (DRS)

The UV−Vis diffuse reflection spectra of raw material, intermediate and final product are presented in Fig. 6. Compared with TiO_2 powders, the protonated titanates show stronger absorption intensity, indicating that the introduction of H^+ and the formation of tubular structure lower the energy gap [18] and hence expand the light spectrum response range. Owing to the stronger electronegativity of Zn, the band gap of $ZnTiO_3$ is narrower than the protonated titanates [31], resulting in the improvement of absorption intensity in the visible light region and obvious redshift. Therefore, the photocatalytic activity of $ZnTiO_3$ is enhanced. The direct optical band gap estimated from the absorption spectra for the unique chain-like $ZnTiO_3$ is shown in Fig. 6. An optical band gap is obtained by plotting $(\alpha h\upsilon)^2$ vs $h\upsilon$, where α is the absorption coefficient and $h\upsilon$ is photon energy. Extrapolation of the linear portion at $(\alpha h\upsilon)^2=0$ gives the band gap of 2.99 eV for the $ZnTiO_3$ material. Thus, for our chain-like $ZnTiO_3$, the minimum energy required for the excitation of an electron from valence to conduction band is lower than that for the pure anatase TiO_2 and ZnO (about 3.2 eV).

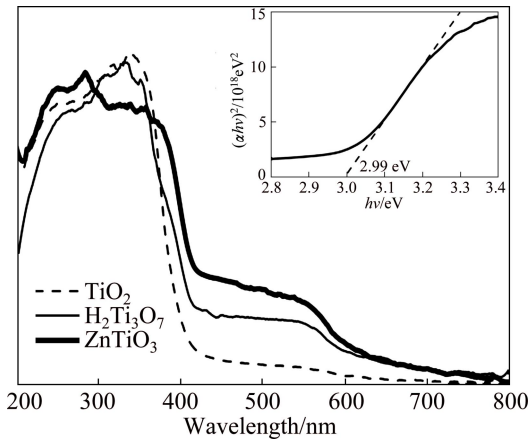

Fig. 6 DRS for TiO_2, $H_2Ti_3O_7$ and $ZnTiO_3$ (inset shows estimated band gap of chain-like $ZnTiO_3$)

3.4 Photocatalytic activity of $ZnTiO_3$

The photocatalytic activity of as-prepared $ZnTiO_3$ was further evaluated by the degradation of aqueous methyl orange under xenon light irradiation. The concentration of the photocatalyst varied from 0.1 to 0.5 g/L. A blank experiment was carried out to test the degradation effect of xenon light. As shown in Fig. 7, the degradation rate of methyl orange solution (10 mg/L) reaches 56.7% in 20 min under the irradiation of xenon light without adding any photocatalyst, which indicates that xenon light presents photocatalytic property.

However, the degradation rate showed obvious increase after adding $ZnTiO_3$ photocatalyst. The photocatalytic degradation rate was enhanced with the concentration of $ZnTiO_3$ increasing from 0.1 to 0.5 g/L, because both the active sites on catalyst surface and the absorption of light by the catalyst increased with the increase of catalyst quantity. The shapes of three curves were similar with each other because the reaction process was related to the initial concentration of methyl orange and light strength [32]. When the concentration of $ZnTiO_3$ was 0.3 g/L, 95.3% methyl orange was removed in 20 min under xenon light irradiation, so the rest of the experiments were carried out in this concentration. In order to further evaluate the degradation ability of the obtained chain-like $ZnTiO_3$, the degradation efficiency of methyl orange was compared with the standard photocatalyst P25. As shown in Fig. 7, the degradation rate is 87.8% under the same reaction condition when the concentration of P25 was 0.3 g/L. The result indicates that the photocatalytic performance of the chain-like $ZnTiO_3$ is slightly better than that of P25. The photocatalytic activity of P25 is similar to the result of Ref. [33].

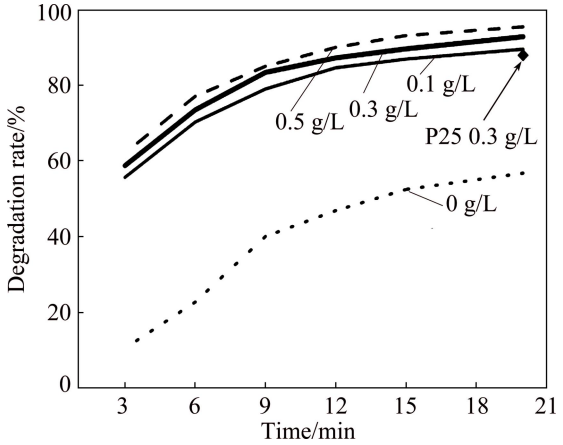

Fig. 7 Effect of $ZnTiO_3$ concentration on degradation rate of methyl orange and comparison with commercial catalyst P25

The effect of initial concentration of methyl orange solution on the photocatalytic process was examined. The reactions of dye decomposition were carried out in the range of 5−15 mg/L. As shown in Fig. 8, the photocatalytic activity of $ZnTiO_3$ showed a big difference with the initial concentration of methyl orange solution varied from 5 to 15 mg/L. It can be observed that the photocatalytic degradation rate decreases as the initial concentration of methyl orange solution increases. The degradation rate reached 99.3%, when the dye concentration was 5 mg/L. The photocatalytic degradation of aromatic compounds was related to the formation of hydroxyl radicals [34], which were formed by the reaction of holes with adsorbed OH^- and H_2O. When the concentration of methyl orange increased, the generation of ·OH would be reduced since there were only fewer sites available for the adsorption of OH^-.

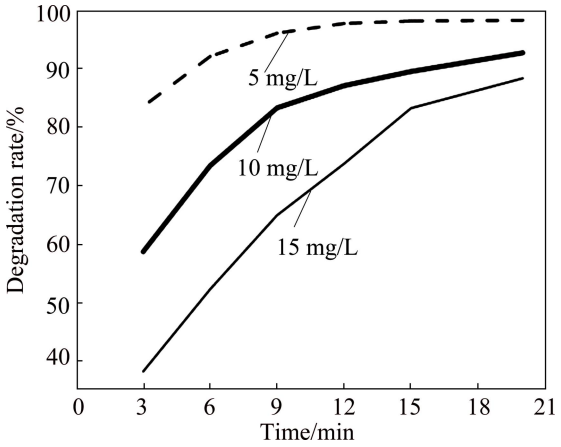

Fig. 8 Effect of initial methyl orange concentration on degradation rate of methyl orange

The photocatalytic degradation generally follows a Langmuir−Hinshelwood mechanism [35]. The kinetics curve of the reaction of 15 mg/L methyl orange solution degradated by 0.3 g/L $ZnTiO_3$ is shown in Fig. 9. After fitting, the equation is $\ln(c_0/c)=0.5557+0.1020t$ (R=0.99012). It indicates that the degradation reaction can be expressed by the first order reaction kinetic model and the rate constant is 0.1020.

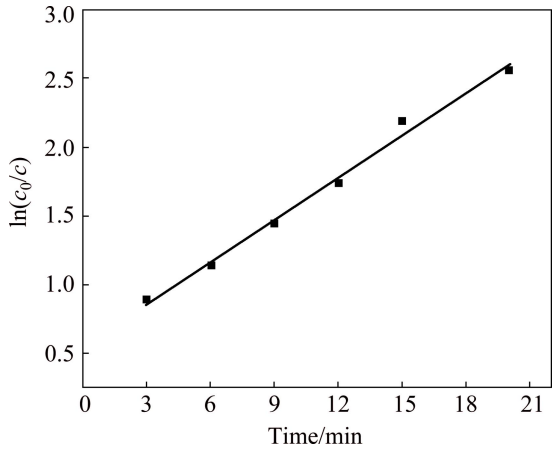

Fig. 9 Kinetics curve of photocatalyst degradation

3.5 Photocatalytic mechanism

In general, the photocatalytic cycle comprises three steps. Firstly, when irradiated under the simulated solar light, the electrons of $ZnTiO_3$ were excited from the valence band (VB) to the conduction band (CB), leaving an equal number of vacant sites (holes). In this step, owing to the stronger electronegativity of Zn, the band gap of $ZnTiO_3$ is narrower than the protonated titanates [31], resulting in the improvement of absorption intensity in the visible light region and obvious redshift,

which makes it easier for the excitation of electrons; Secondly, the excited electrons and holes migrate to the surface. In this step, a large proportion of electron−hole pairs recombine, dissipating the input energy in the form of emitted light. The Zn^{2+} ions act as electron traps retarding electron−hole recombination and enhance interfacial hole transfer to degrade the organic dye adsorbed on the surface of the particles; Thirdly, the photoinduced electrons of the CB could be transferred to the dissolved oxygen to form superoxide anion radicals ($O_2\cdot^-$), which subsequently transform to active oxygen species, such as $HO_2\cdot$, ·OH and H_2O_2. On the other hand, the remaining holes at the valence band of $ZnTiO_3$ reacted with adsorbed water or surface hydroxyl groups (—OH^-) to produce ·OH radicals [36]. These ·OH radicals and the holes were responsible for the degradation of methyl orange. The major initial steps in the mechanism under visible irradiation are summarized by Eqs. (2)−(6).

$$ZnTiO_3+h\nu \longrightarrow e+h^+ \quad (2)$$

$$e+O_2 \longrightarrow O_2\cdot^- \quad (3)$$

$$O_2\cdot^-+H_3O^+ \longrightarrow \cdot OH+HO_2\cdot+H_2O_2 \quad (4)$$

$$h^++H_2O/OH^- \longrightarrow \cdot OH+H^+ \quad (5)$$

$$\cdot OH \text{ or } h^+ + \text{azo dye} \longrightarrow \text{degradation} \quad (6)$$

4 Conclusions

1) The chain-like perovskite $ZnTiO_3$ nanocomposites have been synthesized by the ion-exchange method combined with a hydrothermal process, which is used to prepare the as-synthesized nanostructured $H_2Ti_3O_7\cdot 3H_2O$ with a layered and tubular structure.

2) The introduction of Zn ions enhanced the stability of titanate nanotubes and could avoid damaging the titanate nanotube structure. The unique morphology was transformed from titanate nanotubes. This change in morphology made the surface area larger and enhanced the surface properties. The procedures meet the criteria for effective industrial application. The described procedure might also be used to prepare other perovskite composite oxides.

3) The chain-like $ZnTiO_3$ material exhibited excellent performance on the photocatalytic degradation of methyl orange in a short time, making it a potential alternative for removal of azo dyes in wastewater.

References

[1] LI Zhen-min, ZHANG Peng-yi, LI Jin-ge, SHAO Tian, WANG Juan, JIN Ling. Synthesis of In_2O_3 porous nanoplates for photocatalytic decomposition of perfluorooctanoic acid (PFOA) [J]. Catalysis Communications, 2014, 43: 42−46.

[2] YAO Mao-hai, TANG You-gen, ZHANG Li, YANG Hai-hua, YAN Jian-hui. Photocatalytic activity of CuO towards HER in catalytic from oxalic acid solution under simulated sunlight irradiation [J]. Transactions of Nonferrous Metals Society of China, 2010, 20(10): 1944−1949.

[3] MAQBOOL A, HUSSAIN A, RAHMAN J U, PARK J K, PARK T G, SONG J S, KIM M H. Ferroelectric and piezoelectric properties of $SrZrO_3$-modified $Bi_{0.5}Na_{0.5}TiO_3$ lead-free ceramics [J]. Transactions of Nonferrous Metals Society of China, 2014, 24(S): sl46−sl51.

[4] SUNTIVICH J, GASTEIGER H A, YABUUCHI N, NAKANISHI H, GOODENOUGH J B, YANG S H. Design principles for oxygen-reduction activity on perovskite oxide catalysts for fuel cells and metal–air batteries [J]. Nature Chemistry, 2011, 3: 546−550.

[5] DULIN F H, RASE D E. Phase equilibria in the system ZnO−TiO_2 [J]. Journal of the American Ceramic Society, 1960, 43: 125−131.

[6] ZHANG Q L, YANG H, ZOU J L, WANG H P. Sintering and microwave dielectric properties of LTCC-zinc titanate multilayers [J]. Materials Letters, 2005, 59: 880−884.

[7] LIU Gang, LI Guang-she, QIU Xiao-qing, LI Li-ping. Synthesis of ZnO/titanate nanocomposites with highly photocatalytic activity under visible light irradiation [J]. Journal of Alloys and Compounds, 2009, 481: 492−497.

[8] YADAV B C, YADAV A, SINGH S, KAMAN S. Nanocrystalline zinc titanate synthesized via physicochemical route and its application as liquefied petroleum gas sensor [J]. Sensors and Actuators B: Chemical, 2013, 177: 605−611.

[9] HUANG Jie-jie, ZHAO Jian-tao, WEI Xiao-fang, WANG Yang, BU Xue-peng. Kinetic studies on the sulfidation and regeneration of zinc titanate desulfurization sorbent [J]. Powder Technology, 2008, 180: 196−202.

[10] BARTRAM S F, SLEPETYS R A. Compound formation and crystal structure in the system ZnO−TiO_2 [J]. Journal of the American Ceramic Society, 1961, 44: 493−499.

[11] ZHANG Jin-cang, XU Yan, CAO Shi-xun, CAO Gui-xin, ZHANG Yu-feng, JING Chao. Kondo-like transport and its correlation with the spin-glass phase in perovskite manganites [J]. Physical Review B, 2005, 72: 054410.

[12] YU You-hua, XIA Meng. Preparation and characterization of $ZnTiO_3$ powders by sol−gel process [J]. Materials Letters, 2012, 77: 10−12.

[13] FEI D Q, HUDAYA T, ADESINA A A. Visible-light activated titania perovskite photocatalysts: Characterisation and initial activity studies [J]. Catalysis Communications, 2005, 6: 253−258.

[14] AGEH V, MOHSENI H, SCHARF T W. Lubricious zinc titanate coatings for high temperature applications [J]. Surface and Coatings Technology, 2013, 137: 241−247.

[15] SHROUT T R, HALLIVAL A. Preparation of lead-based ferroelectric relaxors for capacitors [J]. American Ceramic Society Bulletin, 1987, 66: 704−711.

[16] BAVYKIN D V, WALSH F C. Kinetics of alkali metal ion exchange into nanotubular and nanofibrous titanates [J]. The Journal of Physical Chemistry C, 2007, 111: 14644−14651.

[17] HODOS M, H E, HASPEL H, KUKOVECZ Á, KóNYA Z, KIRICSI I. Photosensitization of ion-exchangeable titanate nanotubes by CdS nanoparticles [J]. Chemical Physics Letters, 2004, 399: 512−515.

[18] SUN Xiao-ming, LI Ya-dong. Synthesis and characterization of ion-exchangeable titanate nanotubes [J]. Chemistry—A European Journal, 2003, 9: 2229−2238.

[19] SUN Xi-ping, ZHANG Ji-wei, ZHANG Guo-liang, PAN Xiao-xue, HUANG Tao. Preparation and characteristics of TiO_2 nanotube catalysts used in hybrid photocatalysis/membrane process [J]. Catalysis Communications, 2012, 18: 76−80.

[20] KASUGA T, HIRAMATSU M, HOSON A, SEKINO T, NIIIHARA K. Formation of titanium oxide nanotube [J]. Langmuir, 1998, 14: 3160−3163.

[21] KITANO M, WADA E, NAKAJIMA K, SHIGENOBU H, HAYASHI S, KOBAYASHI H, HARA M. Protonated titanate nanotubes with Lewis and Brønsted acidity: Relationship between nanotube structure and catalytic activity [J]. Chemistry of Materials, 2013, 25: 385−393.
[22] SUZUKI Y, YOSHIKAWA S. Synthesis and thermal analyses of TiO_2-derived nanotubes prepared by the hydrothermal method [J]. Journal of Materials Research, 2004, 19: 982−985.
[23] NAKAHIRA A, KATO W, TAMAI M, ISSHIKI T, NISHIO K, ARITANI H. Synthesis of nanotube from a layered $H_2Ti_4O_9{\cdot}H_2O$ in a hydrothermal treatment using various titania sources [J]. Journal of Materials Science, 2004, 39: 4239−4245.
[24] KITANO M, NAKAJIMA K, KONDO J N, HAYASHI S, HARA M. Protonated titanate nanotubes as solid acid catalyst [J]. Journal of the American Chemical Society, 2010, 132: 6622−6623.
[25] ZHANG S, PENG L M, CHEN Q, DU G H, DAWSON G, ZHOU W Z. Formation mechanism of $H_2Ti_3O_7$ nanotubes [J]. Physical Review Letters, 2003, 91: 256103.
[26] LI N, ZHANG L D, CHEN Y Z, FANG M, ZHANG J X, WANG H M. Highly efficient, irreversible and selective ion exchange property of layered titanate nanostructures [J]. Advanced Functional Material, 2012, 22: 835−841.
[27] ALEXANDER R, THOMAS B, SLAVICA S, BERNADI J, ERICH K, OLIVER D. Charge separation in layered titanate nanostructures: Effect of ion exchange induced morphology transformation [J]. Angewandte Chemie International Edition, 2008, 47: 1496−1499.
[28] YANG J, SWISHER J H. The phase stability of $Zn_2Ti_3O_8$ [J]. Materials Characterization, 1996, 37: 153−159.
[29] ZHANG Min, JIN Zhen-sheng, ZHANG Jing-wei, GUO Xin-yong, YANG Jian-jun, LI Wei, WANG Xiao-dong, ZHANG Zhi-jun. Effect of annealing temperature on morphology, structure and photocatalytic behavior of nanotubed $H_2Ti_2O_4(OH)_2$ [J]. Journal of Molecular Catalysis A: Chemical, 2004, 217: 203−210.
[30] KRYLOVA G, BRIOUDE A, SORAYA A G, MRAZEK J, SPANHEL L. Natural superhydrophilicity and photocatalytic properties of sol−gel derived $ZnTiO_3$−ilmenite/r-TiO_2 films [J]. Physical Chemistry Chemical Physics, 2010, 12: 15101−15110.
[31] ENG H W, BARNES P W, AUER B M, WOODWARD P M. Investigations of the electronic structure of d^0 transition metal oxides belonging to the perovskite family [J]. Journal of Solid State Chemistry, 2003, 175: 94−109.
[32] WANG Shao-bin. A comparative study of Fenton and Fenton-like reaction kinetics in decolourisation of wastewater [J]. Dyes and Pigments, 2008, 76: 714−720.
[33] TIAN Bao-zhu, ZHANG Jin-long, TONG Tian-zhong, CHEN Feng. Preparation of Au/TiO_2 catalysts from Au(I)−thiosulfate complex and study of their photocatalytic activity for the degradation of methyl orange [J]. Applied Catalysis B: Environmental, 2008, 79: 394−401.
[34] SAKTHIVEL S, NEPPOLIAN B, SHANKAR M V, ARABINDOO B, PALANICHAMY M, MURUGESAN V. Solar photocatalytic degradation of azo dye: Comparison of photocatalytic efficiency of ZnO and TiO_2 [J]. Solar Energy Materials and Solar Cells, 2003, 77: 65−82.
[35] LACHHEB H, PUZENAT E, HOUAS A, KSIBI M, ELALOUI E, GUILLARD C, HERRMANN J M. Photocatalytic degradation of various types of dyes (Alizarin S, Crocein orange G, Methyl red, Congo red, Methylene blue) in water by UV-irradiated titania [J]. Applied Catalysis B: Environmental, 2002, 39: 75−90.
[36] LIU Xuan-neng, TANG Yan-hong, LUO Sheng-lian, WANG Yao, ZHANG Xi-lin, CHEN Yao, LIU Cheng-bin. Reduced graphene oxide and $CuInS_2$ co—decorated TiO_2 nanotube arrays for efficient removal of herbicide 2,4—dichlorophenoxyacetic acid from water [J]. Journal of Photochemistry and Photobiology A: Chemistry, 2013, 262: 22−27.

高光催化活性 $ZnTiO_3$ 的合成与表征

严 欣[1]，赵翠连[1]，周义龙[1]，吴振军[1]，袁剑民[2]，李文生[1]

1. 湖南大学 化学化工学院，长沙 410082；
2. 湖南大学 材料科学与工程学院，长沙 410082

摘 要：采用先水热处理法制得钛酸盐纳米管再进行离子交换的两步工艺合成钙钛矿型 $ZnTiO_3$。钛酸盐纳米管成分为 $H_2Ti_3O_7{\cdot}3H_2O$。XRD 测试结果表明，$ZnTiO_3$ 具有立方相钙钛矿结构。SEM 和 TEM 观察到 $ZnTiO_3$ 具有独特的串珠状微观形貌结构。紫外−可见漫反射光谱表明，$ZnTiO_3$ 在可见光区吸收率明显增强。当溶液中 $ZnTiO_3$ 质量浓度为 0.3 g/L 时，在氙灯下照射 20 min，浓度为 15 mg/L 的甲基橙溶液降解率达 95.3%，所得 $ZnTiO_3$ 显示出比相同反应条件下标准催化剂 P25 更高的催化活性。甲基橙的降解动力学符合一级动力学方程，降解反应的速率常数为 0.1020。

关键词：钛酸锌；离子交换；光催化；钙钛矿；合成；表征

(Edited by Yun-bin HE)